Hindawi
Advances in Materials Science and Engineering
Volume 2019, Article ID 7480618, 13 pages
https://doi.org/10.1155/2019/7480618

Research Article

Corrosion Resistance of DLC Film-Coated SUS316L Steel Prepared by Ion Beam Enhanced Deposition

Bei B. Han,[1] Dong Y. Ju,[2,3,4] Mao R. Chai,[2,5] Hui J. Zhao,[3] and Susumu Sato[6]

[1]*Department of Electronic Engineering, Graduate School of Engineering, Saitama Institute of Technology, Fusaiji 1690, Fukaya, Saitama 369-0293, Japan*
[2]*Department Advanced Science Institute, Saitama Institute of Technology, Fusaiji 1690, Fukaya, Saitama 369-0293, Japan*
[3]*Hangzhou Dianzi University, No. 1, 2nd Street Jianggan District, Hangzhou 310000, China*
[4]*Ningbo Institute of Materials Industry Innovation, No. 12, Lane 689, Changxing Road, Jiangbei, Ningbo 315000, China*
[5]*State Power Investment Corporation, Building 3, No. 28, Financial Street, Xicheng District, Beijing 100000, China*
[6]*Department of Information System, Saitama Institute of Technology, Fusaiji 1690, Fukaya, Saitama 369-0293, Japan*

Correspondence should be addressed to Dong Y. Ju; dyju@sit.ac.jp

Received 8 September 2019; Revised 5 November 2019; Accepted 8 November 2019; Published 23 November 2019

Academic Editor: Lingxue Kong

In order to improve the conductivity and anticorrosive resistance of bipolar plates in fuel cells, the characterizations and corrosion behaviors of the DLC-coated SUS316L steel deposited with different gas ratios CH_4/H_2 and deposition times were investigated and evaluated. The chemical bonding structure and composition of the DLC coatings were confirmed by Raman spectroscopy and X-ray photoelectron spectroscopy (XPS). The micromorphology and surface roughness of the DLC were observed by scanning electron microscopy (SEM) and atomic force microscopy (AFM). The element compositions of cross section were determined by electron probe microanalysis (EPMA). The interfacial contact resistance (ICR) was measured. Furthermore, the DLC-coated SUS316L steel was corroded by potentiostatic polarizations in a 0.5 M H_2SO_4 solution at 0.8 V, 90°C for 168 h, and the corrosion behaviors were investigated in the solution using electrochemical techniques. In addition, the metal ions in sulfuric acid corrosion solution were detected by inductively coupled plasma-atomic emission spectroscopy. The results indicate that the DLC coatings deposited at a lower gas ratio CH_4/H_2 of 1 : 1 could result in a decreasing ID/IG ratio of 1.03, low Ra roughness of 3.77 nm, low ICR of 12.9 mΩ cm^2, and low metal ion concentration of 16.60 ppm in the corrosion solution. The significant improvement in the anticorrosion resistance of the DLC film was mainly due to the increased sp^3 element and formation of the passive film. As a result, the DLC coating deposited on the SUS316L steel at $CH_4/H_2 = 1:1$ has better anticorrosion properties. However, the DLC film-coated SUS316L steel still cannot meet the corrosive resistance of the bipolar plate.

1. Introduction

Recently, the more efficient and cleaner energy technologies have been attracted extensive attention. Fuel cells convert chemical energy directly into electrical energy, meanwhile they are environmentally friendly [1]. Polymer electrolyte membrane fuel cell (PEMFC) is one of the most potential energy devices for residential and commercial applications, which are efficient and virtual zero-emissions [2]. As an important component of the PEMFC stack, the bipolar plate plays an important role in providing the electrical contact and transporting current from neighbouring cells, distributing air evenly to the gas diffusion layer-electrode assembly and removing heat and liquid from the active areas [3]. However, the bipolar plates have the disadvantage of high weight, volume, and high expensive cost. Therefore, it is necessary to reduce the cost, volume, and weight of the bipolar plate for the development of PEMFCs [4]. Meanwhile, bipolar plate should have high anticorrosion resistance, low interfacial contact resistance (ICR), low weight, low-volume high mechanical manufacturability, and so on [5].

As the traditional bipolar plate material, graphite has the advantage of high electronic conductivity and excellent

chemical stability in fuel cells. But, it is fragile to impact and it has the disadvantage such as high manufacture costs of gas flow channels and large volume because of its brittleness [6]. The stainless steel has the advantages of high volumetric resistance and mechanical strength, low gas permeability, and economic to manufacture in fuel cells. Its easy machining and shaping properties result in a low volume. Therefore, the metal bipolar plates such as stainless steel, aluminium, and titanium are ideal candidates and commercially available compared with graphite [7]. But, the metal bipolar plate is prone to corrosion in strong acidic fuel cell condition of the electrolyte membrane with a pH value of about 2-3 [8]. Titanium shows better corrosion behavior and higher mechanical properties but more expensive cost than stainless steels. Aluminium is not as good as stainless steel and titanium due to its higher corrosion rate and shorter life. The dissolved metal ions, generated from corrosion, can poison the active sites of the polymeric electrolyte membrane resulting in decreased power output of the PEMFC [8].

To overcome these drawbacks, depositing a protective coating on the metallic bipolar plate is necessary by various surface modification techniques. Some studies have been researched to prevent the bare metal bipolar plates from being corroded by acidic fuel cell environment. Oladoye et al. [9] pointed out that PTFE- (polytetrafluoroethylene-) alumina coatings deposited on the aluminium alloy using the CoBlast process exhibited about a twofold increase in the polarisation resistance of the AA3003 alloy substrate. The suitability of PTFE-coated stainless steel and titanium for use in a PEMFC environment was explored by Baroutaji et al. [10] who described that PTFE coating improved the corrosion resistance but increased the ICR of the coated metals due to the unconductive nature of such coating. Fu et al. [11] reported the carbon coatings on SUS316L substrates by pulsed-bias arc ion plating (PBAIP). They found the excellent performance such as low ICR, high anticorrosion resistance, and high contact angle of the coating with water compared with contact angle of the bare sample with water substrate. Zhang et al. [12] showed that the structure of DLC coating deposited on 316L stainless steel, CoCrMo alloy, and Ti6Al4V substrate by filtered cathode vacuum arc (FCVA) was similar, and the DLC coating revealed a higher corrosion potential and a lower corrosion current than the bare metal substrate. Toro et al. [13] employed DLC film prepared by plasma-enhanced chemical vapor deposition (PECVD) as the barrier coating against corrosive environment and showed that hydrogen variation was the key factor affecting the DLC film resistance by evaluating the correlations between protective behavior and microstructural properties at the atomic scale. Ye et al. [14] researched the tribocorrosion mechanisms of the 304L substrate and multilayer DLC-coated 304L by magnetron sputtering technology in seawater and manifested that the multilayer DLC coating emerged a better antitribocorrosion properties under different potentials. Compared with the other coating techniques, the ion beam enhanced deposition (IBED) method has many advantages such as lower compressive stress due to the production of a graded interfacial, higher film-substrate adhesion, better surface properties of high-precision parts, and selective surface modification, which enables a series of beneficial surface property modifications without detrimentally affecting the bulk properties [15]. Because the IBED augmenting ion beam is controlled independently, film properties such as the interfacial adhesion, density, grain size, and morphology as well as internal stresses can be optimized [16]. The difference between IBED and physical vapor deposition method is that the reactants are delivered individually to the surface directly in the IBED process. The energy of the reaction is supplied by the kinetic energy of ions instead of the plasma temperature, which provides more control over the reaction process and more flexibility in the film properties. Then, an alloyed bond layer is formed to promote adhesion of the film. Film-substrate adhesion is achieved without the external application of heat, and the deposition temperature can be held below 93°C (200°F) [17]. The DLC films generated by precursor CH_4 with higher H/C ratio exhibit a higher diamond structure [18]. The addition of H_2 gas leads to a denser film structure and a smoother surface by attaching and passivating the dangling carbon bonds [19]. Wu et al. [20] studied the effects of flow ratio of H_2 and CH_4 on the structure of DLC coatings. The H_2/CH_4 ratio of 1 : 1 led to a higher adhesion.

In this paper, SUS316L substrates were coated with amorphous hydrogenated carbon (a-C : H) coatings using IBED technique. The characterizations and corrosion behaviors of the DLC-coated SUS316L deposited with different gas ratios CH_4/H_2 and deposition times were investigated and evaluated. Furthermore, the chemical bonding structure and composition of a-C : H films were evaluated. The purpose of this paper is to analyze the anticorrosion property of the DLC-coated SUS316L substrate.

2. Materials and Methods

The DLC films, formed by a-C : H, were deposited onto the SUS316L (Cr 18 wt.%, Ni 12 wt.%, Mo 1.3 wt.%, C 0.01 wt.%, and balanced Fe) using gas CH_4 and H_2 by IBED technology. Overall, the deposition mechanism is complex. In ion beam deposition process, the hydrocarbon gas is ionized and extracted through a grid by an accelerating voltage. Then, the ionized hydrocarbon ions are accelerated to form ion beam. Several reactions, electron-neutral, ion-neutral, and neutral-neutral reactions, are taken place in plasma. These different species of positive ions, radicals, and other hydrocarbons are generated in these reactions. There are several surface processes such as adsorption, desorption, direct incorporation of ions, reemission of H, ion-induced incorporation of neutral radicals, adsorbed layer reactions, surface etching reactions, and sputtering in the species deposition of the DLC film [21]. The neutral species promote DLC film growth due to the ion mass deposition rate [19]. The most species in plasma and these species that contribute more to DLC growth are CH_5^+ and CH_3^+ ions. The schematic diagram of IBED process is illustrated in Figure 1 [17]. The film comprises a fully dense coating and a ballistically bonded zone, i.e., a permeation layer. In the IBED process, high-energy ions mix the initial atom layers of the film

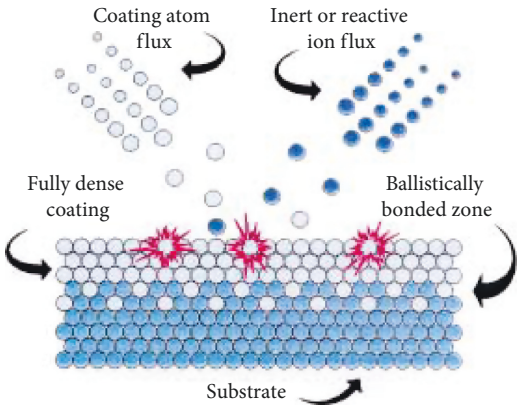

Figure 1: Schematic diagram of IBED process.

material into the surface being coated. It forms an alloyed bond layer which improves coating adhesion and allows coatings to be applied to virtually any substrate without an intermediate layer. The coating grows from the alloyed layer and the high-energy ion flux controls the coating's grain structure, density, and residual stresses [16].

These substrates with size of 100 mm (L) × 100 mm (W) × 0.1 mm (H) were ultrasonically cleaned in acetone for 15 min to remove the grease contamination from the surface. Prior to the deposition, the chamber was evacuated to a base pressure of 4×10^{-4} Pa for producing plasma discharge. Then, CH_4 and H_2 mixture was injected into the chamber, and the pressure was fixed at 2×10^{-3} Pa. The gas flow, accelerating current, and voltage were fixed at 0.4-0.5 sccm, 2.5 mA, and 10 kV for all the samples. At last, the DLC coatings were deposited on the SUS316L successfully. All the samples were cooled down inside the chamber after processing. Four types of coatings were formed in this paper (Table 1).

The chemical bonding structure and composition of the DLC coatings were confirmed by NRS-4100 Raman spectroscopy using the laser wavelength of 532.0 nm and Physical Electronics (PHI) Quantum 2000 X-ray photoelectron spectroscopy (XPS) using a monochromatic Al-Kα X-ray source with an energy of 1486.6 eV, operating at 13 kV and 12 mA. The chamber pressure was fixed at $\sim 1.33 \times 10^{-7}$ Pa. The pass energy was set to 20 eV to make sure high resolution and high sensitivity. The micromorphology and surface roughness of the coatings were observed and evaluated using scanning electron microscopy (SEM) and SPM-9500J3 atomic force microscopy (AFM). The cross section used for SEM was milled by a focused ion beam (FIB) with a JIB-4500 multibeam system. The element compositions of the cross section polished with a diamond paste (0.05 μm) were determined by an electron probe microanalysis (EPMA) JXA-8900R. The ICR of the specimen was evaluated by a similar way on previous studies [22].

At last, the DLC-coated SUS316L was corroded by potentiostatic polarizations in 0.5 M H_2SO_4 at 90°C for 168 h. The schematic diagram of corrosion test is shown in Figure 2. The metal ions in the sulfuric acid corrosion solution were detected by inductively coupled plasma (ICP)

Table 1: Parameters of various processing conditions.

Substrate	SUS316L			
CH_4/H_2	1 : 1		1 : 0	
Deposition time	6 h	12 h	6 h	12 h

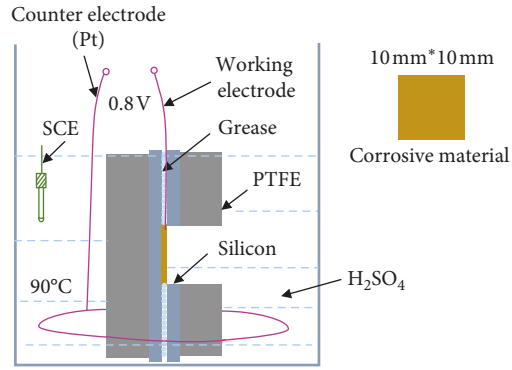

Figure 2: Schematic diagram of corrosion test.

atomic emission spectroscopy after the corrosion experiment. The electrochemical behaviors of all samples were analyzed in 0.5 M sulfuric acid solution at 90°C by the conventional three-electrode system. The DLC-coated SUS316L sample was acted as the working electrode, a platinum sheet as the counter electrode, and a saturated calomel electrode (SCE) as the reference electrode. The sample was cut to a size of 20×20 mm^2 by a circular saw after the deposition, and then sealed with epoxy resin and exposed one end with an area of 10×10 mm^2.

3. Results and Discussion

3.1. Surface Morphology. AFM measurements are carried out for uncoated SUS316L (a) and DLC films deposited at (b) $CH_4/H_2 = 1:1$, 6 h; (c) $CH_4/H_2 = 1:1$, 12 h; (d) $CH_4/H_2 = 1:0$, 6 h; and (e) $CH_4/H_2 = 1:0$, 12 h as shown in Figure 3. From these figures, it can be seen that the undulating hills with a height of about 138.00 nm, 44.86 nm, 67.95 nm, 39.97 nm, and 65.51 nm appear on the surface of bare and DLC films, respectively. The Ra roughness of uncoated SUS316L and the DLC film-coated SUS316L is 21.80 nm, 3.77 nm, 5.63 nm, 3.93 nm, and 7.56 nm, respectively. The surface of the DLC film deposited at 6 h becomes more flattened than that of the DLC film deposited at 12 h. This can be explained by considering that the deposition process prevails on the etching phenomena: the high-energy ion beams continuously bombard the surface with the increase of time, etching away the interfacial and unstable carbon atoms belonging to the still un-relaxed domains [13, 16].

The cross-section morphology of the DLC film is observed by SEM. The cross-section morphology images of the DLC film deposited on SUS316L at (a) $CH_4/H_2 = 1:1$, 6 h; (b) $CH_4/H_2 = 1:1$, 12 h; (c) $CH_4/H_2 = 1:0$, 6 h; and (d) $CH_4/H_2 = 1:0$, 12 h are presented in Figure 4. The DLC films on the surface are very dense. The thickness of the fully dense coating cannot be clearly defined because of the permeation

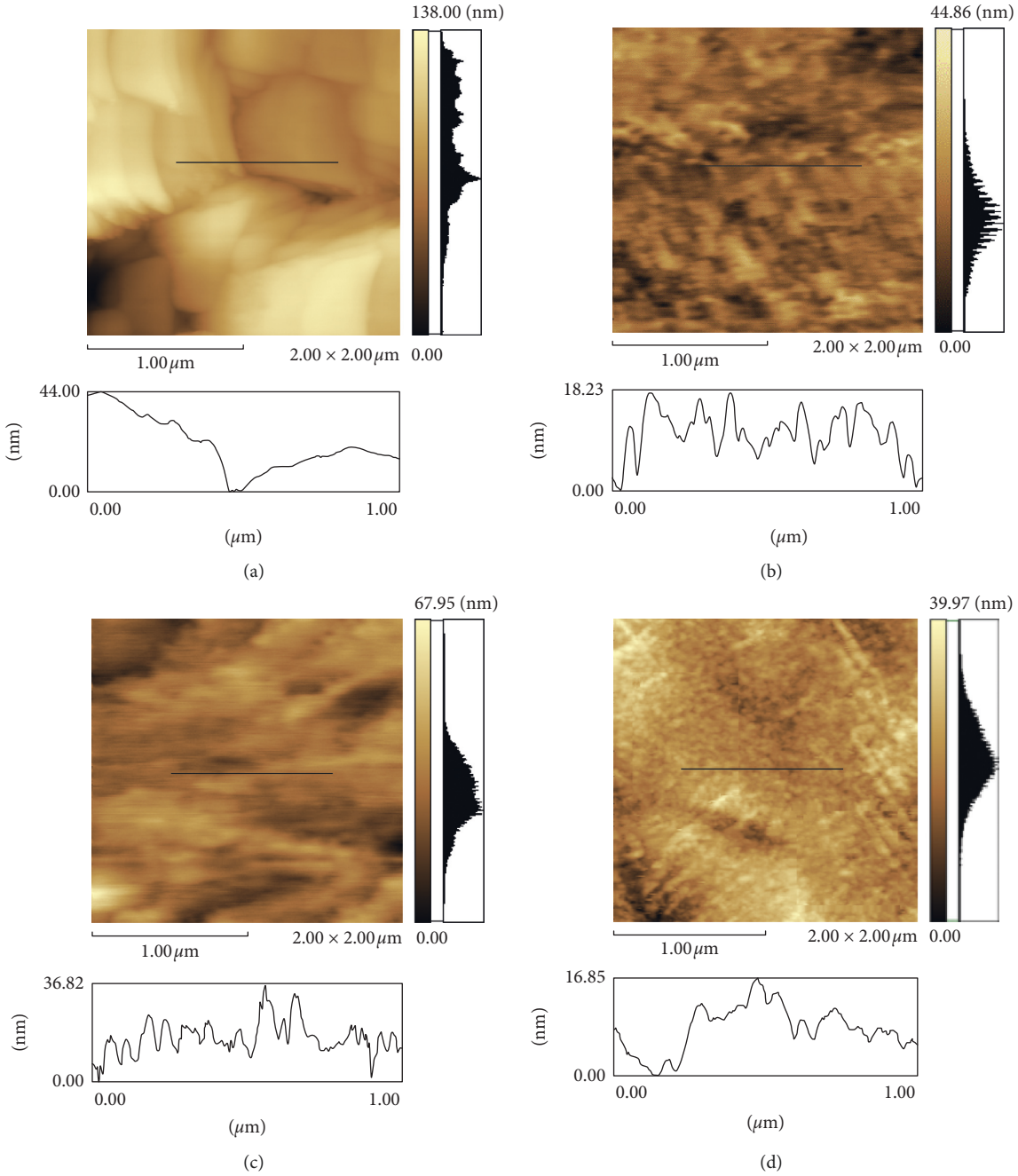

Figure 3: Continued.

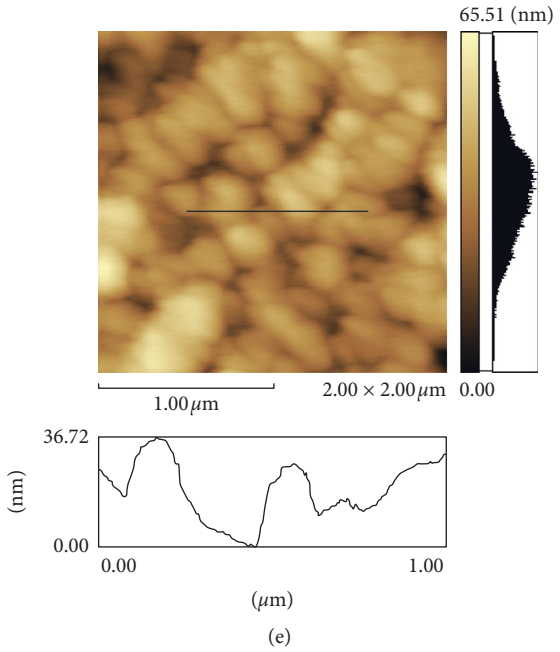

FIGURE 3: AFM 2D images and linear *Z*-axis scale bars of uncoated SUS316L (Ra = 21.80 nm) (a) and DLC coatings deposited at (b) $CH_4/H_2 = 1:1$, 6 h (Ra = 3.77 nm); (c) $CH_4/H_2 = 1:1$, 12 h (Ra = 5.63 nm); (d) $CH_4/H_2 = 1:0$, 6 h (Ra = 3.93 nm); (e) $CH_4/H_2 = 1:0$, 12 h (Ra = 7.56 nm).

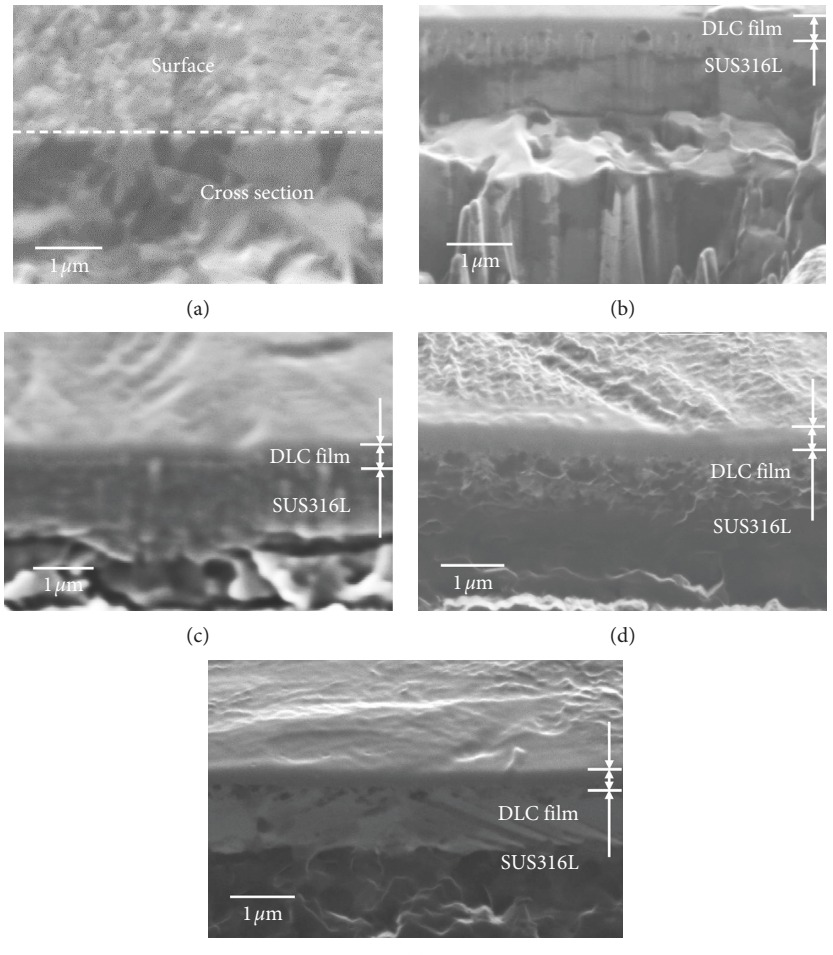

FIGURE 4: Cross-section SEM image at a rotated angle of 52° of uncoated SUS316L (a) and the DLC film deposited at $CH_4/H_2 = 1:1$, 6 h (b); $CH_4/H_2 = 1:1$, 12 h (c); $CH_4/H_2 = 1:0$, 6 h (d); $CH_4/H_2 = 1:0$, 12 h (e).

layer. The DLC layer has a maximum thickness of the fully dense coating of about 569.8 nm from Figure 4(b). The average thickness of the fully dense coating is about 543.4 nm, 543.3 nm, and 407.6 nm, respectively, from Figures 4(c)–4(e). With the increase of time, the high-energy ion beams continuously bombard the growing film, and the surface desorption process plays a dominant role. So, the coating atoms are penetrated into the substrate with more energy, which reduces the thickness of the fully dense coating and increases the thickness of the permeation layer [16].

The carbon element concentration distribution of DLC film-coated SUS316L was determined by EPMA. The sample to be analyzed was bombarded by an electron beam which would emit X-rays with wavelengths characteristic to specific elements. Then, the concentration distribution and diffusivities of elements could be obtained accurately by EPMA mapping [23, 24]. The average thickness of the carbon permeation layer is about 25 μm, 8 μm, and 7 μm, respectively, from Figure 5(b), 5(f), and 5(h). The liner scan of carbon is not significantly reduced in Figure 5(d), so the thickness is estimated to be 35 μm combined with the carbon concentration distribution (Figure 5(c)). The limited lateral resolution may also reduce the accuracy of the results. The liner scans indicate that the carbon concentration decreases with the distance. The thickness of the DLC film deposited on the SUS316L substrate at the condition of gas ratio $CH_4/H_2 = 1:1$ is thicker than that of $CH_4/H_2 = 1:0$. As the increase of deposition time, the penetration depth of DLC increases because of the increase in the high-energy ion beam, but the intensity of carbon weakens. The coating atoms are penetrated into the substrate with more energy to reduce the thickness of the fully dense coating and increase the thickness of the permeation layer at the deposition time of 12 h.

3.2. Raman Spectroscopy. The chemical bonding structure was characterized by Raman spectroscopy because it is nondestructive. The Raman feature of DLC coating has been explained previously [18, 25]. The G (graphite) peak is resulted from the stretching mode of sp^2 sites (both olefinic and aromatic), while D (disorder) peak results from the breathing mode of sp^2 sites (only aromatic) [26]. The position of G-peak and the ratio of D-peak to G-peak (ID/IG) are the important factors which fully depend on the structure of DLC coating. In order to extract these factors, the Raman spectrum of DLC coating was decomposed to two Gaussian peaks (D-peak to G-peak). Figure 6 exhibits the typical Raman spectra of DLC films deposited on SUS316L. The spectrum displays a broad asymmetric Raman scattering band in the range of 1000–2000 cm^{-1}, representing typical features of carbon coating.

Raman features such as ID/IG ratio and G-peak position are specifically shown in Table 2. The Raman shift error exists due to factors such as the pixel of detector, laser wavelength accuracy, and the fitting by a Gaussian method [27]. The variation of G-peak position toward higher Raman shift shows that the chemical bonding is changed from olefinic to aromatic. The G-peak position is changed from 1558 to 1570 cm^{-1} by decreasing the CH_4 ratio and the deposited time for the SUS316L substrate. Moreover, the decreased ID/IG shows an increase in size and number of clusters, a decrease in chain-like structures [19, 28]. ID/IG ratio of the DLC film deposited on SUS316L at gas ratio $CH_4/H_2 = 1:1$, 6 h is 1.03, meanwhile ID/IG of DLC coating deposited at gas ratio $CH_4/H_2 = 1:0$, 6 h is 1.21. Meanwhile, the G-peak position is shifted from 1558.45 to 1568.85 cm^{-1} indicating the increase in sp^2-C content. In a-C : H coating, a decrease in ID/IG corresponds to a decrease in sp^2/sp^3. Therefore, the DLC film deposited at $CH_4/H_2 = 1:1$, 6 h has a higher sp^3 content with a diamond-like tetrahedral structure which leads to a better anticorrosion resistance [29].

3.3. XPS Analysis. The C 1s XPS profiles of DLC films deposited on SUS316L are shown in Figure 7. The strong amorphous carbon peaks at 284.6 eV and 285.6 eV are identified to represent sp^2-C and sp^3-C bonding indicating that the DLC coating is deposited on the SUS316L successfully [30]. The surface oxide film on SUS316L having a thickness of 2–4 nm means a very small oxygen content [31]. The DLC film may contain oxygen content and not just from oxidation in the air. The oxygen atomic concentration of DLC films deposited at $CH_4 = 1:1$, 6 h; $CH_4/H_2 = 1:1$, 12 h; $CH_4/H_2 = 1:0$, 6 h; and $CH_4/H_2 = 1:0$, 12 h is about 17.92%, 21.59%, 21.84%, and 27.77%, respectively. It is known that DLC coatings with more C-H bonds and less C=O and C-O bonds (around 286.5 eV) suggesting a denser coating [32]. The gas ratio $CH_4/H_2 = 1:1$ with a higher H/C ratio led to a less graphitic structure (sp^2-C) from Table 2 and Figure 7. It may be due to the interaction between hydrogen and the dangling bonds of carbon during the deposition process. The hydrogen could attach and passivize the dangling carbon bonds. With the increase of time, the high-energy ion beams continuously bombard the growing film, causing sp^3-C to break down into the stable two-dimensional sp^2-C structure.

3.4. Interfacial Contact Resistance. The low ICR is the key factor to obtain high performance for metallic bipolar plates of PEMFCs. The ICR of the SUS316L substrate and DLC films at 150 N/cm^2 is shown in Table 3. The ICR is obtained by subtracting the resistance of the substrate from the resistance of DLC film-coated SUS316L [33]. The good conductive performance depends on high content of sp^2-C bonds. Since the DLC film penetrates into the substrate from EPMA results, the increase of ICR under the condition of $CH_4/H_2 = 1:0$ may be due to an increase of sp^3-C content in the permeation layer. It results that ICR is not in good agreement with the sp^2/sp^3 ratio mentioned above. Therefore, the DLC film-coated SUS316L at $CH_4/H_2 = 1:1$ is available for fuel cells. Nevertheless, the DLC films deposited at $CH_4/H_2 = 1:1$, 12 h showed lowest resistance of 12.9 $m\Omega\,cm^2$ which is still slightly higher than the Department of Energy's (DOE) target (2020) of 10 $m\Omega\,cm^2$ [34].

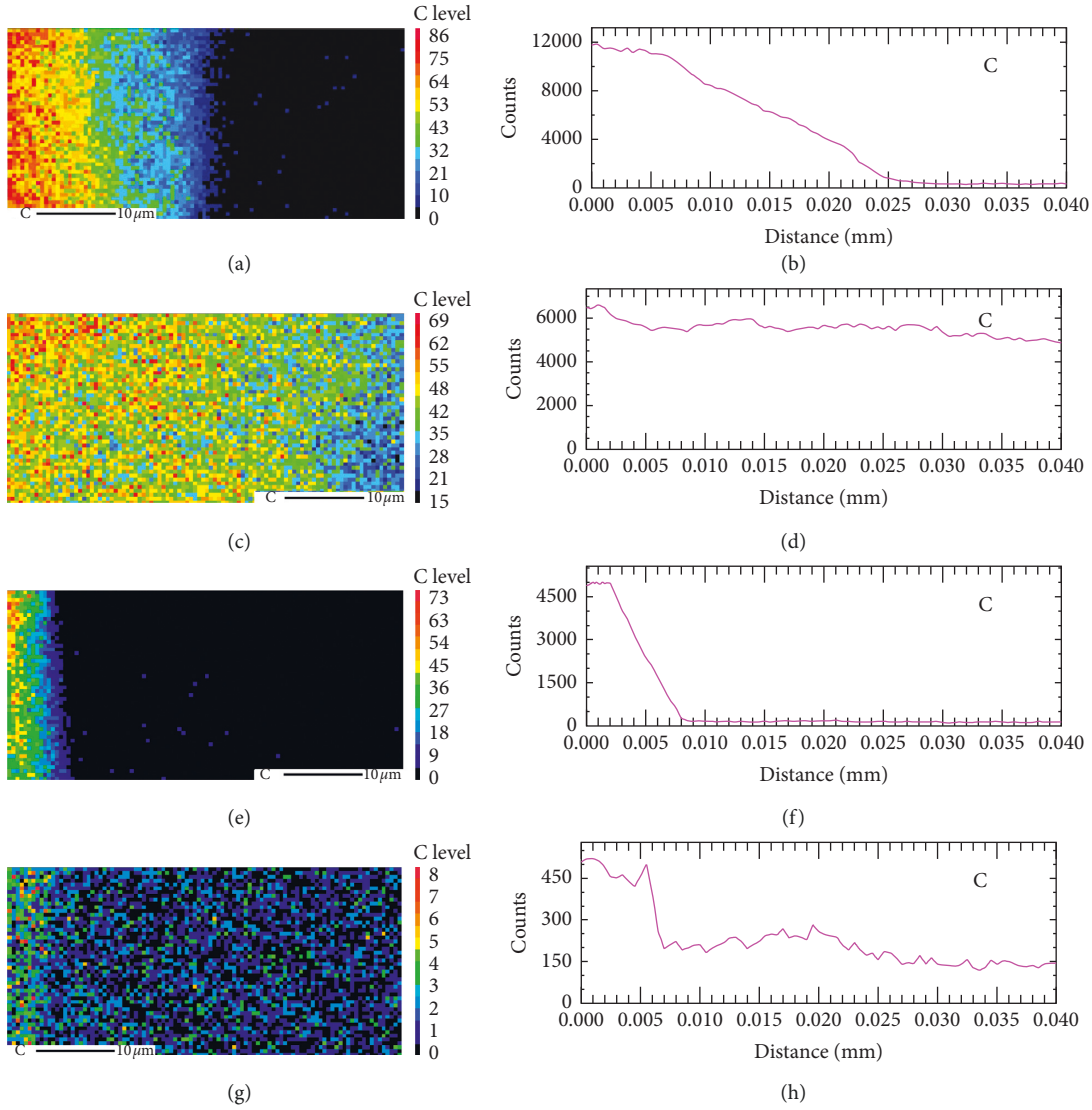

Figure 5: EPMA mappings of carbon element and EPMA line scans of carbon intensity of the DLC film cross section deposited at (a) and (b) $CH_4/H_2 = 1:1$, 6 h; (c) and (d) $CH_4/H_2 = 1:1$, 12 h; (e) and (f) $CH_4/H_2 = 1:0$, 6 h; (g) and (h) $CH_4/H_2 = 1:0$, 12 h.

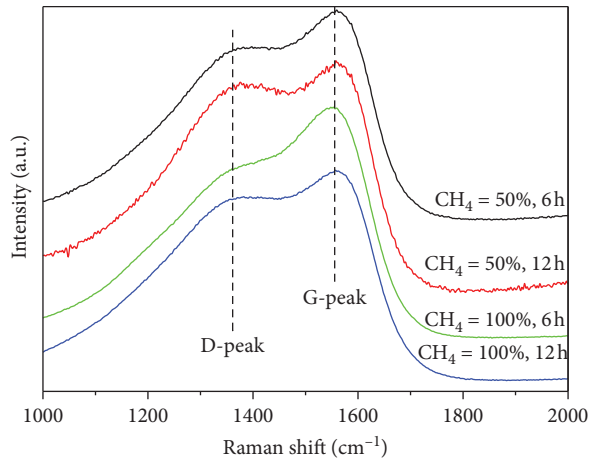

Figure 6: Typical Raman spectrum of DLC coatings deposited on SUS316L at different conditions.

Table 2: Raman features, i.e., ID/IG ratio and G-peak position of different DLC coatings.

Substrate	$CH_4/H_2 = 1:1$ 6 h	$CH_4/H_2 = 1:1$ 12 h	$CH_4/H_2 = 1:0$ 6 h	$CH_4/H_2 = 1:0$ 12 h
I_D/I_G	1.03	1.30	1.21	1.31
G-peak (cm^{-1})	1558.45	1568.91	1568.85	1570.53

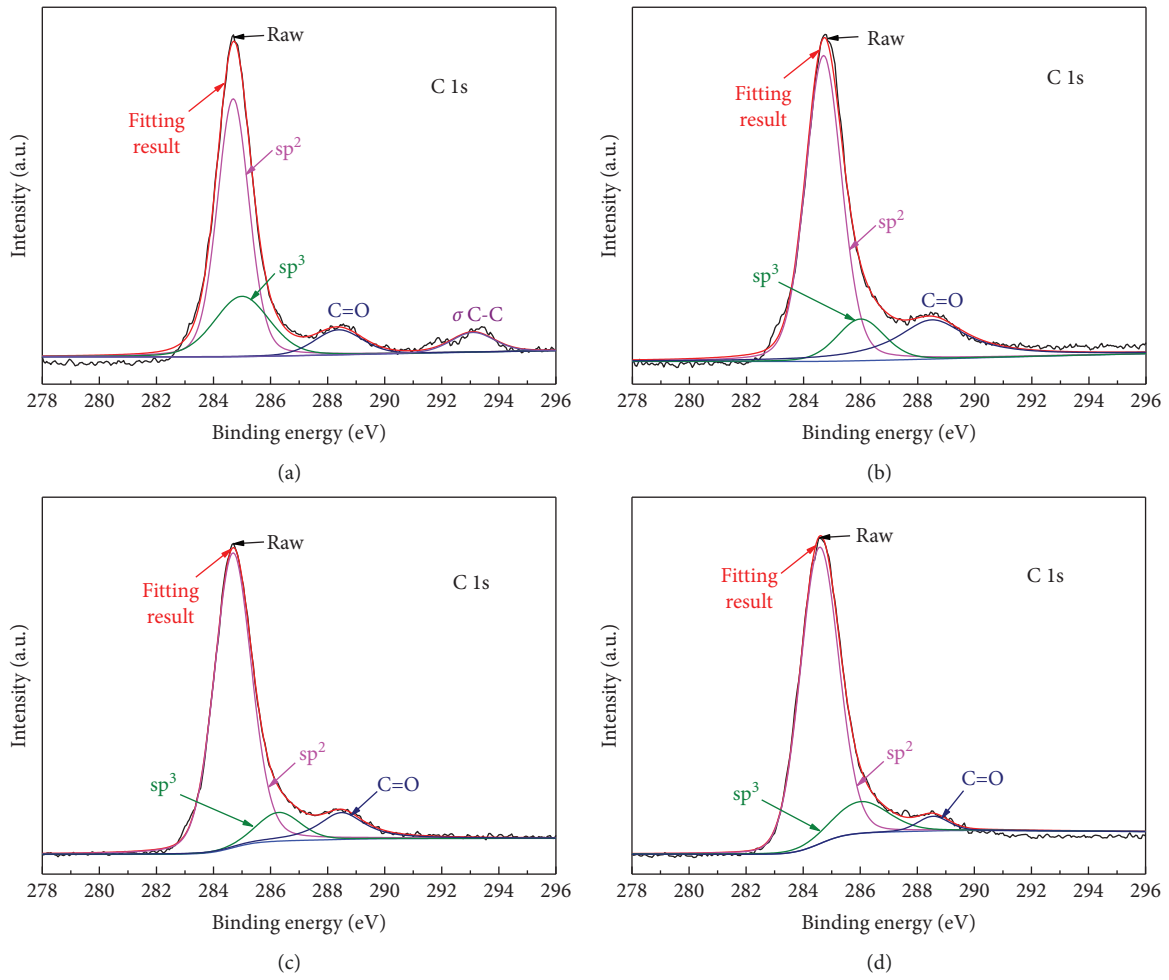

Figure 7: C 1s XPS profiles of DLC films deposited on SUS316L at (a) $CH_4/H_2 = 1:1$, 6 h; (b) $CH_4/H_2 = 1:1$, 12 h; (c) $CH_4/H_2 = 1:0$, 6 h; (d) $CH_4/H_2 = 1:0$, 12 h.

3.5. Corrosion Resistance of DLC Films. Figure 8 shows the surface morphology SEM images of SUS316L (a) and DLC films deposited at (b) $CH_4/H_2 = 1:1$, 6 h; (c) $CH_4/H_2 = 1:1$, 12 h; (d) $CH_4/H_2 = 1:0$, 6 h; and (e) $CH_4/H_2 = 1:0$, 12 h after the corrosion experiment. The cross-section morphology SEM images of SUS316L and different DLC coatings are presented in Figure 9. DLC films are still found on the surface of the substrates, and the thickness of the DLC film is thinner than before from these pictures. It is observed that the DLC films are destroyed in corrosion test, and some cracks appear on the surface. The surface morphology is changed and some larger corrosion pits are observed on the surface at the condition of $CH_4/H_2 = 1:0$, 6 h than those of $CH_4/H_2 = 1:1$, 6 h. The pitting corrosion regions are marked with red circles, as shown in Figure 8. SUS316L constituents like Fe, Cr, and Ni are stable in elemental form below −0.7 V vs. SCE. In the fuel cell operating conditions, SUS316L constituents are stable in the form of Fe^{2+}, Fe^{3+}, Ni^{2+}, and Cr^{3+} oxidized states [34]. In the corrosion test of high temperature acidic solution of 168 hours, a small amount of acidic solution penetrates into the film and contacts with SUS316L. Then, oxide is generated between the substrate and the film, causing the DLC film to rupture and forming pitting corrosion. For the DLC films coated on the SUS316L substrate, a local region is suffered from accelerated corrosion due to the pits.

Figure 10 displays the typical Raman spectrum of DLC films deposited on SUS316L after corrosion test. The G-peak intensity of the DLC film at the condition of $CH_4/H_2 = 1:0$, 6 h is weaker than that of $CH_4/H_2 = 1:1$, 6 h, indicating a

Table 3: ICR for SUS316L and DLC coatings deposited under different conditions.

	Substrate	$CH_4/H_2 = 1:1$ 6 h	$CH_4/H_2 = 1:1$ 12 h	$CH_4/H_2 = 1:0$ 6 h	$CH_4/H_2 = 1:0$ 12 h
ICR ($m\Omega \cdot cm^2$)	35	23.7	12.9	105.9	79.9

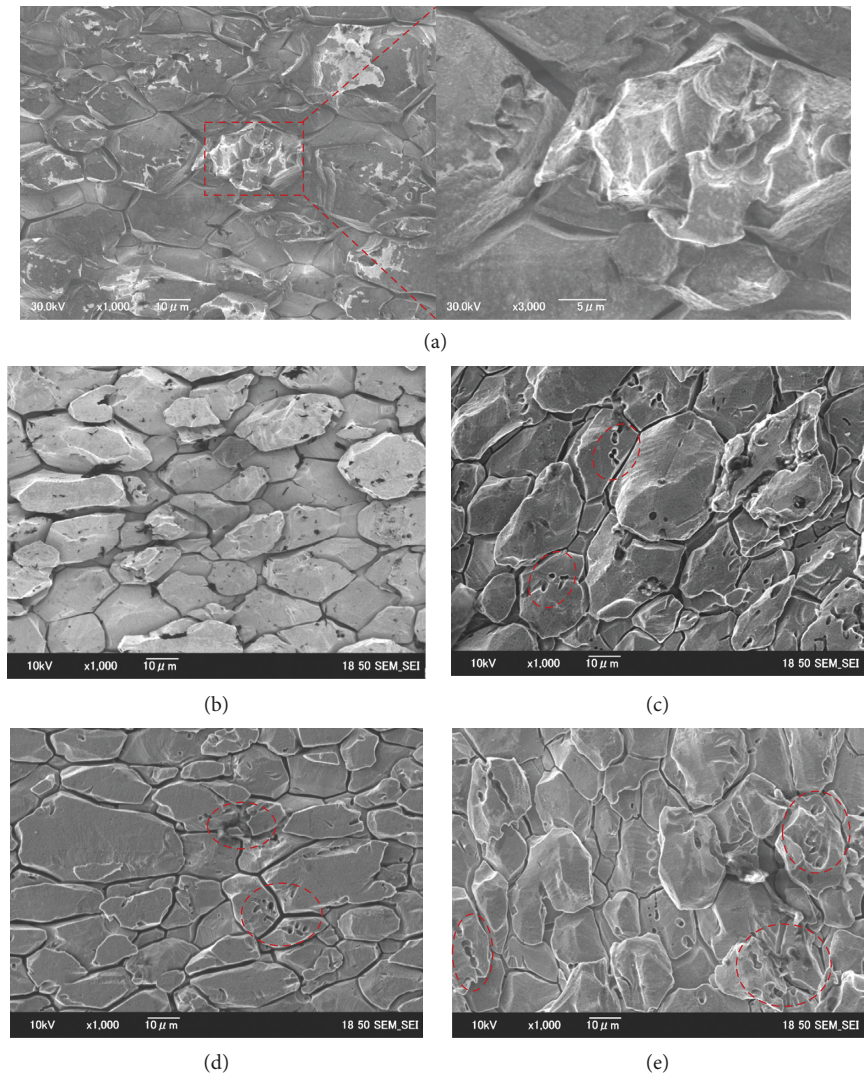

Figure 8: Surface morphology SEM images of SUS316L (a) and DLC coatings deposited at $CH_4/H_2 = 1:1$, 6 h (b); $CH_4/H_2 = 1:1$, 12 h (c); $CH_4/H_2 = 1:0$, 6 h (d); $CH_4/H_2 = 1:0$, 12 h (e) after corrosion test.

reduction of sp3-C ratio. Therefore, the DLC film deposited at $CH_4/H_2 = 1:1$, 6 h has the better corrosion resistance.

Metal ion concentration in the corrosion solution is important for evaluating the corrosive resistance of the bipolar plate. Hence, metal ion concentration for the bare and DLC film-coated SUS316L after 168 h corrosion test is summarized in Table 4. Compared to the concentration of the uncoated substrate, the metal ions leached from DLC film-coated SUS316L have a significant reduction with a minimum of 16.60 ppm, indicating that the DLC films play an important role in protecting the substrate. The main reason is that there is an easily corroded place on the surface of the DLC film coated on SUS316L. The pitting reaction takes place in the passivation film formed on SUS316L due to the self-excited reaction, and some pores are formed on the substrate [35]. In addition, there are hydrogen ions in the corrosive solution, forming a strong corrosion layer and accelerating the corrosion rate [36], meanwhile, intergranular corrosion cracking inside the SUS316L. All of these have a destructive effect on the DLC film coated on the SUS316L. From Table 4, the DLC film deposited at the condition of $CH_4/H_2 = 1:1$, 6 h has a lower concentration than that of $CH_4/H_2 = 1:0$, 6 h because the DLC film deposited at $CH_4/H_2 = 1:0$, 6 h is relatively thin and not dense enough which can be observed from Figures 4 and 5. The higher

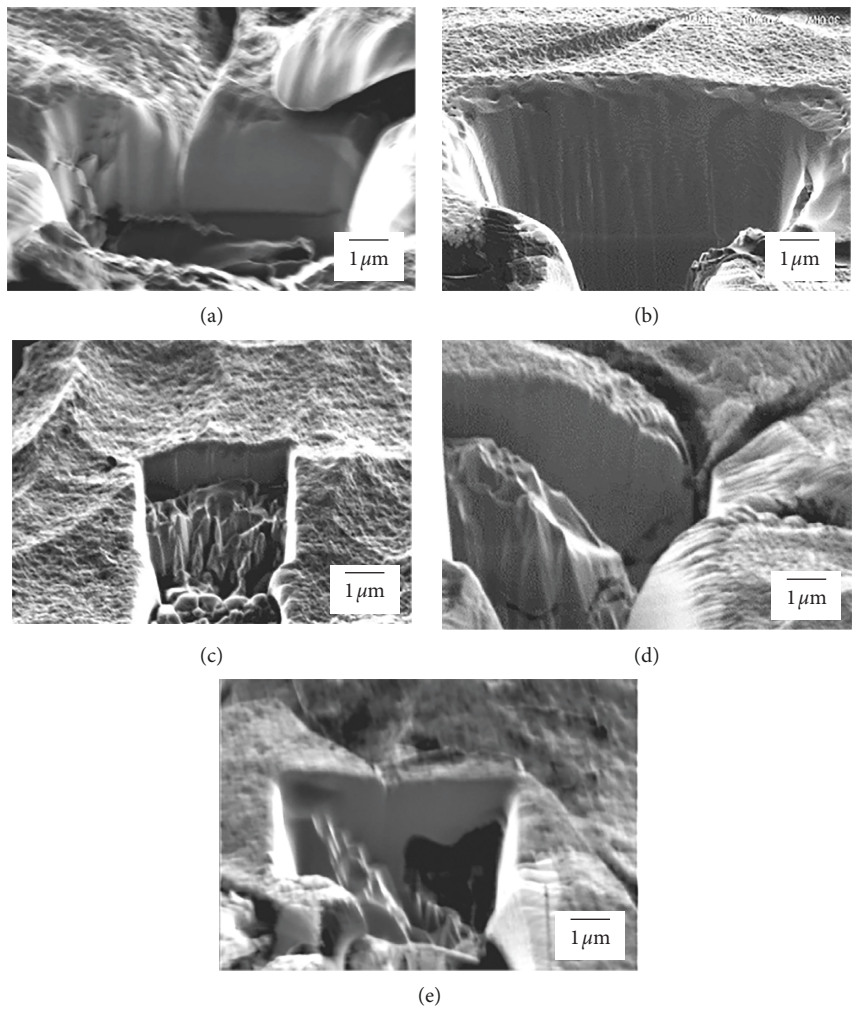

Figure 9: Cross-section SEM images at a rotated angle of 52° of SUS316L (a) and DLC films deposited at $CH_4/H_2 = 1:1$, 6 h (b); $CH_4/H_2 = 1:1$, 12 h (c); $CH_4/H_2 = 1:0$, 6 h (d); $CH_4/H_2 = 1:0$, 12 h (e) after corrosion test.

oxygen content of the DLC film deposited at $CH_4/H_2 = 1:0$ also accelerates corrosion rate in an acidic solution. After 168 h corrosion test, part of the substrate is exposed to the acid corrosion solution, which is more susceptible to corrosion. Meanwhile, the corrosion behavior is consistent with the cross-section SEM images of the DLC coatings showed in Figure 4.

The polarization curves of SUS316L and DLC film-coated SUS316L in the 0.5 M sulfuric acid solution purged with air at 90°C are shown in Figure 11. In comparison with the bare, the DLC film-coated SUS316L exhibits a more noble corrosion potential and more stable passive region in simulated cathode condition. Corrosion potential reaches a maximum of about 0.1 V at the condition of $CH_4/H_2 = 1:1$, 12 h, which is significantly greater than the bare of about −0.2 V. The higher corrosion potential usually implies the better corrosion resistance because of the higher electrochemical stability [5]. At the cathode potential of around 0.6 V under the fuel cell operating condition, the corrosion current density of the bare is about 19 $\mu A/cm^2$. As for the DLC film-coated SUS316L, the corrosion current density is reduced to a minimum of 0.5 $\mu A/cm^2$ at $CH_4/H_2 = 1:1$, 6 h and 12 h. The corrosion current density of DLC films deposited at $CH_4/H_2 = 1:1$ meet the DOE's 2020 target of 1 $\mu A/cm^2$ (0.5 M H_2SO_4 solution with 5 ppm HF, 70°C) [37]. A smaller current density means a lower corrosion rate. All the DLC film-coated SUS316L exhibit the similar passivation behavior. The high active peak could be viewed because of the active dissolution and the oxidation. The passivation film formed on the surface could protect SUS316L from contacting sulfuric acid solution, so as to avoid corrosion. The DLC films deposited at $CH_4/H_2 = 1:1$ have the better electrochemical behavior and higher corrosion resistance due to the intrinsic microstructure properties from the surface morphology, which are in accordance with the ICP results. The polarization behavior under the anode condition was not examined because the corrosion behavior of anode condition would be weak [33].

4. Conclusions

In this paper, the dense and uniform DLC films as the protective film were successfully deposited on SUS316L steel using IBED technique by changing the gas ratio CH_4/H_2 and deposition time. The microstructure and corrosion properties of the films were evaluated taking into account for

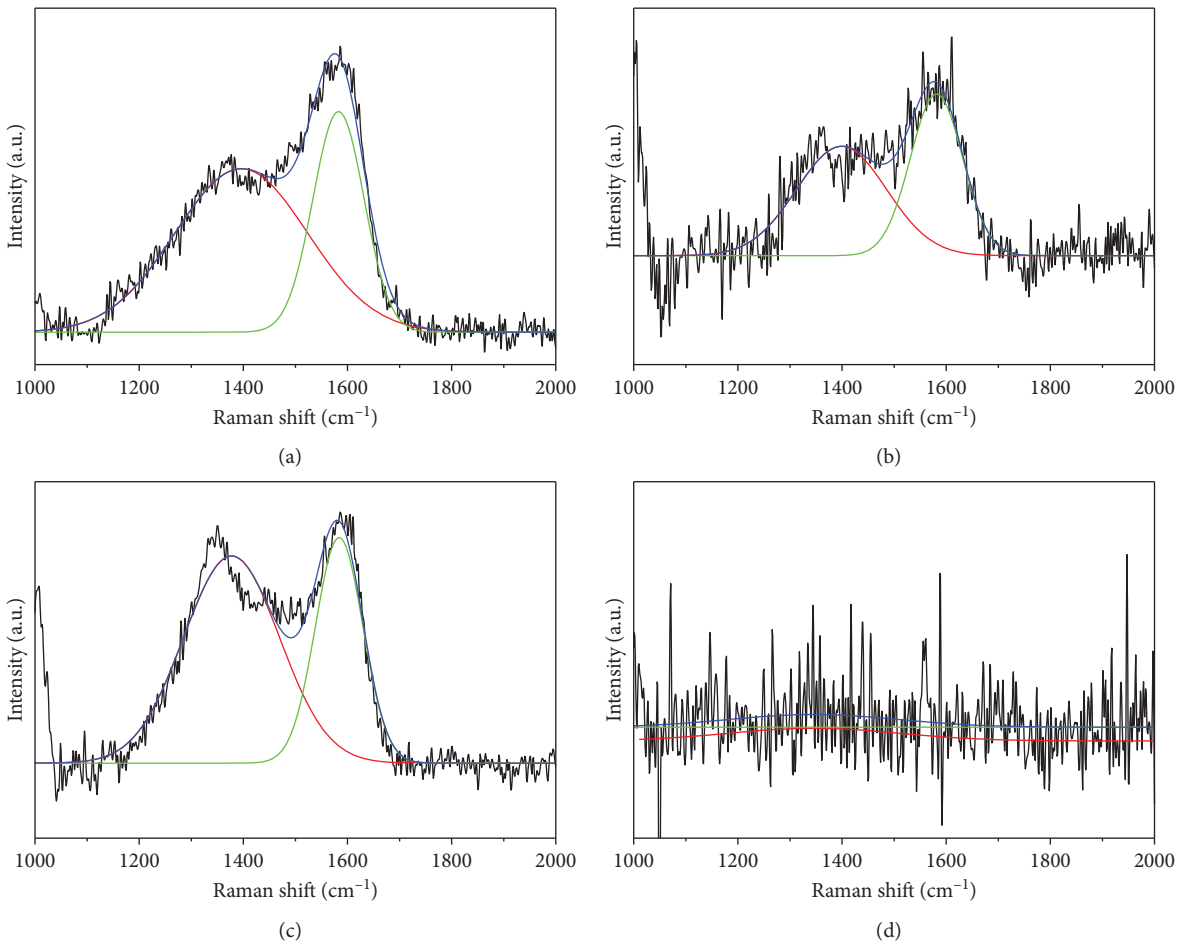

Figure 10: Typical Raman spectrum of DLC films deposited on SUS316L at (a) $CH_4/H_2 = 1:1$, 6 h; (b) $CH_4/H_2 = 1:1$, 12 h; (c) $CH_4/H_2 = 1:0$, 6 h; (d) $CH_4/H_2 = 1:0$, 12 h after corrosion test.

Table 4: Metal ion concentration for the bare and DLC film-coated SUS316L after 168 h corrosion.

	Substrate	$CH_4/H_2 = 1:1$ 6 h	$CH_4/H_2 = 1:1$ 12 h	$CH_4/H_2 = 1:0$ 6 h	$CH_4/H_2 = 1:0$ 12 h
ICP (ppm)	51.72	16.60	25.22	19.56	33.90

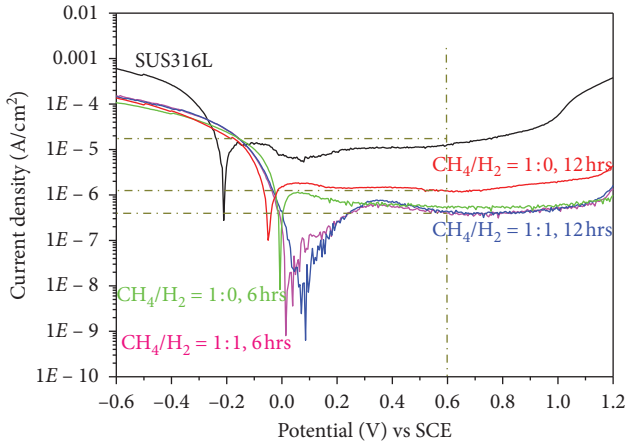

Figure 11: Potentiodynamic behaviors of uncoated SUS316L and various DLC films coated SUS316L in 0.5 M H_2SO_4 at 90°C.

different deposition conditions. We observed that the gas ratio CH_4/H_2 of 1 : 1 contributed to the increase in film thickness and sp^3 bond fraction, resulting in a decrease in corrosion current density and metal ion concentration. Because hydrogen restores the high potential of the oxidic species in the SUS316L surface such as Fe, Cr to the low potential, which results in easier formation of Fe-C, Cr-C bonds on the substrate, improves the adhesion and density between the film and substrate. The metal ion concentration and surface roughness of DLC coating deposited at 6 h are obviously lower than those of DLC deposited at 12 h. The pitting corrosion takes place in the passivation film due to the self-excited reaction, and some pores are formed on the surface to accelerate the corrosion rate. As a result, the DLC film-coated SUS316L steel deposited at CH_4/H_2 of 1 : 1 and deposition time of 6 h has the best corrosion resistance with a dense film thickness of about 569.8 nm and a carbon permeation layer thickness of about 25 μm, indicating the low corrosion current density of 0.5 $\mu A/cm^2$ and low metal ion concentration of 16.60 ppm because of the higher chemical inertness and the few pinholes. The corrosion current density of DLC film-coated SUS316L deposited at $CH_4/H_2 = 1 : 1$ meets the DOE's 2020 target of 1 $\mu A/cm^2$. Nevertheless, the DLC films deposited at $CH_4/H_2 = 1 : 1$, 12 h with the lowest resistance of 12.9 $m\Omega\,cm^2$ is still higher than the DOE's target (2020) of 10 $m\Omega\,cm^2$. Based on these discussions, the DLC films are useful to restrain the corrosion process. However, the DLC film-coated SUS316L steel still cannot meet the resistance of the bipolar plate. Hence, future work would be needed to improve the DLC film-coated SUS316L resistance by adding a conductive path to the DLC film while reducing the cost of the manufacturing.

Data Availability

The data used to support the findings of this study are included within the article.

Conflicts of Interest

The authors declare that there are no conflicts of interest regarding the publication of this paper.

Acknowledgments

This research was funded by State Power Investment Corporation and the Ningbo Institute of Materials Industry Innovation in China.

References

[1] S. R. Dhakate, S. Sharma, and R. B. Mathur, "A low-density graphite-polymer composite as a bipolar plate for proton exchange membrane fuel cells," *Carbon Letters*, vol. 14, no. 1, pp. 40–44, 2013.

[2] J. Hwang, W. Chang, F. Weng, A. Su, and C. Chen, "Development of a small vehicular PEM fuel cell system," *International Journal of Hydrogen Energy*, vol. 33, no. 14, pp. 3801–3807, 2008.

[3] H. Tawfik, Y. Hung, and D. Mahajan, "Metal bipolar plates for PEM fuel cell-A review," *Journal of Power Sources*, vol. 163, no. 2, pp. 755–767, 2007.

[4] H. Wang and J. A. Turner, "Reviewing metallic PEMFC bipolar plates," *Fuel Cells*, vol. 10, no. 4, pp. 510–519, 2010.

[5] K. Feng, X. Cai, H. Sun, Z. Li, and P. K. Chu, "Carbon coated stainless steel bipolar plates in polymer electrolyte membrane fuel cells," *Diamond and Related Materials*, vol. 19, no. 11, pp. 1354–1361, 2010.

[6] N. F. Asri, T. Husaini, A. B. Sulong, E. H. Majlan, and W. R. W. Daud, "Coating of stainless steel and titanium bipolar plates for anticorrosion in PEMFC: a review," *International Journal of Hydrogen Energy*, vol. 42, no. 14, pp. 9135–9148, 2017.

[7] E. A. Cho, U.-S. Jeon, S.-A. Hong, I.-H. Oh, and S.-G. Kang, "Performance of a 1 kW-class PEMFC stack using TiN-coated 316 stainless steel bipolar plates," *Journal of Power Sources*, vol. 142, no. 1-2, pp. 177–183, 2005.

[8] J. R. Mawdsley, J. D. Carter, X. Wang et al., "Composite-coated aluminum bipolar plates for PEM fuel cells," *Journal of Power Sources*, vol. 231, pp. 106–112, 2013.

[9] A. Oladoye, J. Carton, A. Baroutaji et al., "Corrosion and wear resistance of PTFE-Al_2o_3 coatings deposited on aluminum alloy by a microblasting process," in *TMS 2019 148th Annual Meeting & Exhibition Supplemental Proceedings*, pp. 755–762, Springer, Berlin, Germany, 2019.

[10] A. Baroutaji, J. G. Carton, A. M. Oladoye, J. Stokes, B. Twomey, and A. G. Olabi, "Ex-situ evaluation of PTFE coated metals in a proton exchange membrane fuel cell environment," *Surface and Coatings Technology*, vol. 323, pp. 10–17, 2017.

[11] Y. Fu, G. Lin, M. Hou, B. Wu, Z. Shao, and B. Yi, "Carbon-based films coated 316L stainless steel as bipolar plate for proton exchange membrane fuel cells," *International Journal of Hydrogen Energy*, vol. 34, no. 1, pp. 405–409, 2009.

[12] T. F. Zhang, Q. Y. Deng, B. Liu et al., "Wear and corrosion properties of diamond like carbon (DLC) coating on stainless steel, CoCrMo and Ti6Al4V substrates," *Surface and Coatings Technology*, vol. 273, pp. 12–19, 2015.

[13] R. G. Toro, P. Calandra, B. Cortese et al., "Argon and hydrogen plasma influence on the protective properties of diamond-like carbon films as barrier coating," *Surfaces and Interfaces*, vol. 6, pp. 60–71, 2017.

[14] Y. Ye, Y. Wang, X. Ma, D. Zhang, L. Wang, and X. Li, "Tribocorrosion behaviors of multilayer PVD DLC coated 304L stainless steel in seawater," *Diamond and Related Materials*, vol. 79, pp. 70–78, 2017.

[15] P. Sioshansi and E. J. Tobin, "Surface treatment of biomaterials by ion beam processes," *Surface and Coatings Technology*, vol. 83, no. 1–3, pp. 175–182, 1996.

[16] A. H. Deutchman and R. J. Partyka, "Ion beam enhanced deposition," *Advanced Materials and Manufacturing Processes*, vol. 161, pp. 33–35, 2003.

[17] A. H. Deutchman and R. J. Partyka, "Industrial scale ion beam enhanced deposition (IBED) processing system," in *ASM International Surface Engineering Congress*, ASM International, Cleveland, OH, USA, 2002.

[18] J. Ortiz-Medina, H. Kitano, A. Morelos-Gomez et al., "Nanostructured carbon-based membranes: nitrogen doping effects on reverse osmosis performance," *NPG Asia Materials*, vol. 8, no. 4, p. e258, 2016.

[19] J. Robertson, "Diamond-like amorphous carbon," *Materials Science and Engineering: R: Reports*, vol. 37, no. 4–6, pp. 129–281, 2002.

[20] J. L. Wu, H. Zhou, J. Zheng, L. M. Yang, Y. S. Zhang, and H. J. Hu, "Effects of flow ratio of H_2 and CH_4 on structure and

friction properties of hydrogen diamond-like carbon films," *China Surface Engineering*, vol. 28, pp. 42–48, 2015.

[21] J. Martí-González and E. Bertran, "Mechanical and surface characterization of diamond-like carbon coatings onto polymeric substrate," 2015, https://arxiv.org/abs/1509.08512.

[22] H. Wang, M. A. Sweikart, and J. A. Turner, "Stainless steel as bipolar plate material for polymer electrolyte membrane fuel cells," *Journal of Power Sources*, vol. 115, no. 2, pp. 243–251, 2003.

[23] J. H. Kim, J. T. Yeom, J. K. Hong, S. Y. Shim, S. G. Lim, and N. K. Park, "Effect of scandium on the hot extrudability of 7075 aluminum alloy," *Metals and Materials International*, vol. 16, no. 4, pp. 669–677, 2010.

[24] W. Lengauer and M. Bohn, "Thermochemical basis of the preparation of well-defined transition metal carbide, nitride and carbonitride reference materials for electron-probe microanalysis (epma)," *Solid State Phenomena*, vol. 274, pp. 20–42, 2018.

[25] B. Han, D. Ju, S. Sato, and H. Zhao, "Plasma preparation method and tribological properties of diamond-like carbon coating on magnesium alloy AZ_{31} substrate," *Science China Technological Sciences*, vol. 62, no. 11, pp. 1939–1947, 2019.

[26] T. Santra, T. Bhattacharyya, P. Patel, F. Tseng, and T. Barik, "Diamond, diamond-like carbon (DLC) and diamond-like nanocomposite (DLN) thin films for MEMS applications," in *Microelectromechanical Systems and Devices*, N. Islam, Ed., pp. 460–466, InTech, Rijeka, Croatia, 2012.

[27] C. Casiraghi, A. C. Ferrari, and J. Robertson, "Raman spectroscopy of hydrogenated amorphous carbons," *Physical Review B*, vol. 72, no. 8, Article ID 085401, 2005.

[28] W. Dai, X. Gao, J. Liu, S.-H. Kwon, and Q. Wang, "Compositionally modulated multilayer diamond-like carbon coatings with AlTiSi multi-doping by reactive high power impulse magnetron sputtering," *Applied Surface Science*, vol. 425, pp. 855–861, 2017.

[29] N. B. Huang, H. Yu, L. S. Xu, S. Zhan, M. Sun, and D. W. Kirk, "Corrosion kinetics of 316L stainless steel bipolar plate with chromiumcarbide coating in simulated PEMFC cathodic environment," *Results in Physics*, vol. 6, pp. 730–736, 2016.

[30] K. Furlan, A. Klein, and D. Hotza, "Diamond-like carbon films deposited by hydrocarbon plasma sources," *Reviews on Advanced Materials Science*, vol. 34, pp. 165–172, 2013.

[31] T. Hanawa, S. Hiromoto, A. Yamamoto, D. Kuroda, and K. Asami, "XPS characterization of the surface oxide film of 316L stainless steel samples that were located in quasi-biological environments," *Materials Transactions*, vol. 43, no. 12, pp. 3088–3092, 2002.

[32] M. Yoshida, T. Tanaka, S. Watanabe, M. Shinohara, J.-W. Lee, and T. Takagi, "Improvement of oxygen barrier of PET film with diamond-like carbon film by plasma-source ion implantation," *Surface and Coatings Technology*, vol. 174-175, pp. 1033–1037, 2003.

[33] T. Fukutsuka, T. Yamaguchi, S.-I. Miyano, Y. Matsuo, Y. Sugie, and Z. Ogumi, "Carbon-coated stainless steel as PEFC bipolar plate material," *Journal of Power Sources*, vol. 174, no. 1, pp. 199–205, 2007.

[34] R. A. Autunes, M. C. L. Oliveira, G. Ett, and V. Ett, "Corrosion of metal bipolar plates for PEM fuel cells: a review," *International Journal of Hydrogen Energy*, vol. 35, no. 8, pp. 3632–3647, 2010.

[35] A. Kumar, M. Ricketts, and S. Hirano, "Ex situ evaluation of nanometer range gold coating on stainless steel substrate for automotive polymer electrolyte membrane fuel cell bipolar plate," *Journal of Power Sources*, vol. 195, no. 5, pp. 1401–1407, 2010.

[36] H. T. Pan, Q. J. Xu, H. Yun, and X. Q. Deng, "Review on corrosion and surface modification of stainless steel bipolar plates for proton exchange membrane fuel cells," *Corrosion and Protection*, vol. 32, p. 585, 2011.

[37] Technical Plan-Fuel Cells, U.S. Department of Energy, https://www.energy.gov/sites/prod/files/2014/03/f12/fuel_cells.pdf.